

### Author’s reply (AC2) to reviewer #1’s comments (RC1)

First I (the author) would like to thank the anonymous reviewer (#1) for constructive criticism, towards improvement and clear dissemination.

I’ll include the reviewer’s comments as I respond point-by point, starting with the summary and proceeding through the comments.

The reviewer’s comments are indented/italic, including their original numbers.

*“Summary:*

*This paper presents a derivation of the turbulent length scale as a function of standard deviation and wind profile using the Mann model (Mann, 1994) and also closely following the derivations provided in de Mare and Mann (2016). This reviewer believes that the manuscript has potential to be published, but first several clarifications are needed. Please see the full list of my comments below.”*

I would argue that the derivations in this paper **do not** ‘follow’ those in de Mare & Mann (2016). While the new expression (5) can be compared to an analogous one in de Mare & Mann, most of the expressions I derived don’t have any correspondence or equivalent in de Mare & Mann—e.g. the simple practical (and perhaps most important) expression  $L_{MM} \simeq \sigma_u / (dU/dz)$ . I should add that the derivations in this work were done in 2015–16 (except the new generic vonKarman-simplification in eq.7); i.e. the work was done independently and concurrently in a different project than de Mare & Mann (2016).

1. *“After Eq. (3) define  $L_{MM}$  as the turbulent length scale in Mann-model. You described all other parameters except for  $L_{MM}$ .”*

This error due to editing is now corrected in the revision.

2. *“Although this reviewer is not a native English speaker, I would suggest that the authors uses less parentheses and footnotes if possible. For instance, the last sentence in Section 2.1.1 (around Line 20 on Page 4) contains many commas and a semicolon and parentheses that makes it difficult to understand. Similar examples can be found elsewhere in the manuscript.”*

I have attempted to use footnotes in such a way as to preserve the flow of the main text, so that details are available to the interested reader while minimally interrupting the flow.

However, as reviewer #1 points out, there are some relatively convoluted sentences. I have worked to clean up/clarify these in the revision.

3. *“Sometimes you are using Figure and sometimes Fig. for figures (in Section 3.1 and later). Please be consistent.”*

I intentionally use ‘Fig.’ in some passages to avoid overusing the word ‘Figure’ in places where more references to figures occur. Checking the WES manuscript guidelines, this appears to be ok (I’d prefer to leave it, unless WES objects per their English style preferences).

4. *“Font size in your figures is very large. I am not sure if this will be handled in the production stages if the manuscript gets accepted, but if not, you should decrease the font size.”*

Such ‘big’ figures were made for scaling to 1-column width (half of current size) in the final publication.

5. *“Please specify the frequency of the occurrence of wind speeds above  $7\text{ m s}^{-1}$  at the Høvsøre mast. Why  $7\text{ m s}^{-1}$  and not, for instance,  $5\text{ m s}^{-1}$ ?”*

As written/mentioned, this was done with consideration of loads in a concurrent project—given the relatively infrequent occurrence, lower impact on loads, higher difficulty fitting spectra in that regime, and larger spread of results.

Considering winds above cut-in,  $P(U > 7\text{ m s}^{-1})$  for the period analyzed is 66% for the land case and 81% for the offshore case.

I updated the analysis to be for the range 4–25 m/s (where  $U > 7\text{ m/s}$  is noted for its slight difference) and re-made the plots.

The conditional dependence of  $L_{MM}$  on wind speed is beyond the scope of this paper, but is the subject of ongoing work.

6. *“Section 4.1 (Implications and Applications) should not be a part of the concluding section. Conclusions should conclude the study and not elaborate on the applications of the result. Please move Implications and Applications prior to Conclusions and remove the subsection title Summary of conclusions (Section 4.2). It is not typical to have subsections in conclusions.”*

I revise based on your suggestions.

7. *“To this reviewer, current Section 4.1 is a typical discussion section and not implications and applications. I suggest the author renames this section to discussion.”*

I updated to make this part of the discussion section.

8. *“The author concludes (e.g., Line 21 on Page 17) that  $L_{MM}$  is influenced by atmospheric stability but the analyses in this study are not conducted for unstable, stable and neutral conditions separately. Nothing has been said about the fluxes of sensible heat, Richardson number, Obukhov length, etc.*

9. *Related to my previous comment, the paper by Pena Diaz et al. (2010) clearly lists the stability classes that were investigated (Table I in that article), so it would be useful to see similar analysis in this paper.”*

Responding to points 8–9 together: explicit stability considerations are beyond the scope of the current article. Part of the point of this paper is that for application to loads, where one is concerned most with  $\{\sigma_u, U, \alpha, L_{MM}\}$ , which are affected by stability, one then needs to get  $L_{MM}$  (the other 3 are easily obtained). We are not concerned here with stability itself—as the turbines are *not directly affected* by stability, as (re-)stated in the article and references cited.

However, in parallel work (in preparation for publication) and in related recent articles with Chougule et al (cited) we/I have examined treatment of stability.

Again, this is the subject of another paper, particularly because stability does not have a direct affect—but acts through  $\sigma_u, U, \alpha(dU/dz)$  and  $L_{MM}$ .

10. *“Please clarify the purpose of Section 2.2.2 (Modelled spectra: Covariances, anisotropy and  $\Gamma$ ) and Section 2.3 (Ideal, neutral and surface-layer implications). All figures referee [sic] to Eq. (15) and the expressions prior to that equation. I dont see how these sections contribute to the manuscript.”*

Section 2.2.2 shows the theoretical self-consistency of the derived  $\tau_M$  and model, with regard to  $u_*$  (i.e. shear stress) and  $\sigma_u$  and w.r.t. the mixing-length relation. Along the way, §2.2.2 also gives practical/understandable expressions for how Mann-model  $\sigma_u$  and  $u_*$  depend on  $\Gamma$ .

Section 2.3 shows the surface-layer limit of the derived  $L_{MM}$ ; previously it was assumed that the Mann-model is basically designed to work in this limit. Further, §2.3 derives the expected asymptotic (neutral/equilibrium) relation connecting observed  $\sigma_u$  and the model-constraining  $\sigma_{iso}$ .

11. *“Please discuss the reasons why the peak in the Mann model in Figure 6 is not captured by the other two models? This peak, although at small wavenumbers, is very prominent and should be explained.*

*Please discuss.”*

As discussed in the text, this minor peak is not prominent (‘probability well under 1%’). Note Fig. 6 is plotted in log-log coordinates, and these larger  $L_{MM}$  in the minor bump are less than 1/1000 times likely than the values occurring around the major peak. I should adjust ‘under 1%’ to become ‘under 0.1%’.

This minor peak is likely not captured because information related to its cause is not carried through  $dU/dz$ , but rather within horizontal gradients—which implicitly affect the fit parameters including  $L_{MM}$ . I did not wish to speculate, without more detailed measurements; this kind of advective artifact is not trivial to pick apart, given the conditions and the difficulty of fitting spectra to the Mann-model when the observed spectral-peaks are at smaller wavenumbers.

12. *“What is the sampling frequency of the lidar data? The peak in Figure 6 seem not to appear in Figure 5, so is it possible that the lidar measurements contain some bias or some filtering was applied (or something else)?”*

As mentioned above this peak is rather rare and corresponds to the distances to a forest edge. The LIDAR are not the cause, as the peak comes from the sonic anemometer; using data from the sonics only (over smaller vertical extent), the same trend (no peak) arises as when using the LIDAR. Further, the LIDAR and sonic data at 45/44 m are giving values almost identical to each other.

13. *“Please specify the source for Eq. (6).”*

Equation 6 follows from  $\tau_M$  integrated explicitly using the vonKarman spectrum: eq.3 is equal to eq.5. I now add mention of (3) and (5) being equal in the text preceding (6), to avoid confusion.

14. *“I recommend that the author writes the alternative equation for  $L_{MM}$  in Line 27, Page 5 as a numerated equation and not an in-line expression [i.e., Eq. (16)] since some researchers might prefer the usage of turbulence intensity and shear exponent over standard deviation and wind profile (or maybe they already have the data in the form of  $I$  and  $\alpha$ ).”*

Amusingly in an earlier working draft I had actually done this, but removed it, thinking I had too many equations. But I agree and will switch back to having a separate numbered equation for  $L_{MM} \simeq zI_{obs}/\alpha$ .

### **Author’s reply (AC4) to reviewer #2’s comments (RC2)**

The author (MK) would like to thank reviewer #2 for the compliments and constructive suggestions.

Here I will respond to the points raised by the reviewer, copying their points (from their annotation of the draft manuscript) inside quotes using *italic font*, and including page/line numbers:

1. p.1, lines 14–17 “*This looks very useful during the design phase of a wind-farm, particularly offshore.*”

Thanks; I hope it’s useful, and look forward to get more offshore measurements, at ‘taller’ heights, to further verify the model—as I extend it conditionally per wind speed.

2. p.2, lines 6–8 “*While  $L_{MM}$  is certainly one of the central Mann model parameter, anisotropy parameter  $\Gamma$  is also quite important. In the IEC standard, it is recommended to use  $\Gamma = 3.9$ , but its value also varies under different stability conditions. Therefore, I suggest to tone down the ‘the most relevant’ to ‘critical’, so that  $\Gamma$  is not forgotten :-)*”

As mentioned and referenced in the text, Dimitrov and others found that  $L_{MM}$  is more relevant than  $\Gamma$  for modern horizontal-axis turbines (and control systems) analyzed; e.g. Sobol coefficients for  $\Gamma$  have been found to be much smaller than those for  $L_{MM}$ . But there is a (small) possibility that in some circumstance (turbine and/or control system configuration) for some component load that the sensitivity to  $\Gamma$  could be higher than for the turbulence length scale. The variation in  $\Gamma$  is also mentioned, to avoid ‘forgetting’ it as well—the text reads “most relevant load-driving parameters”, and this includes  $\Gamma$ .

But I change ‘relevant’ to ‘crucial,’ inspired by the reviewer’s suggestion.

3. p.2, line 20 (equation 1) “*Please add a reference to this equation.*”

There is no reference for this equation; rather it is a generic finding of the author, which corresponds to/relates all of the different forms of  $\tau$  found in the literature (and referenced). (Such an expression could be useful in the future for e.g. fractal turbulence considerations.)

4. Figures 1–2 (p.8,10) “*Please add a legend indicating magnitude of joint probabilities, which I guess is hidden in the color intensity.*”

Done.

5. p.12, lines 7–10 “*Is Eq. (13) then recommended to use instead of Eq. (15), by using the ratio in the bracket to be 1.11/1.13?*”

The value of 1.11 (or 1.13) corresponds to deviation from  $\langle c_m u_* / \sigma_u \rangle = 1$

for an average including all recorded speeds between 4–25 m/s (or 7–25 m/s). If one wished to consider speeds only above 7 m/s at this site, then one could perhaps approximate the growth of this factor by the ratio 1.13/1.11—but this is found thus far only for this site and wind speed ranges. Later text (following this sentence) explains more about  $\langle c_m u_* / \sigma_u \rangle$ .

6. p.17, line 19 (second bullet-point in summary of conclusions/§4.2) “On page 12 in the last paragraph, it seems that argument is made in favour of the ratio  $>1$ . Therefore, I suggest clarifying this in relation to those statements.”

Note the ratio is ‘ $\approx 1$ ’ in the statement/second bullet point; the statement goes on to say that  $L_{MM}$  can then be approximated by  $\sigma_u / (dU/dz)$ . I have added a sentence to the end of the previous bullet-point, noting that this ratio can be 1–1.11 (or re-directing a reader of only the conclusion to check out the details).

### Author’s reply (AC3) to comments by A. Peña (SC1)

*“Thanks for a very interesting paper. It is indeed extremely convenient to have a parametrization for the Mann length scale that is based on commonly measured parameters. Here three short comments on your manuscript:”*

Thanks; I’m hoping to provide something which is theoretically and empirically sound, and convenient to use in wind applications.

*“1. My previous work both in the citations and in the references should be Peña, A and not Peña Diaz, A. I think you have two references (and the corresponding citations) with that issue.”*

Ok, I’ll update my BibTeX entries that include your name.

*“2. In Peña et al. (2010) we did not explicitly suggest a parametrization for the Mann length scale but we relate it to the length scale of the wind profile as you point out. Your work suggests  $L_{MM} \approx \sigma_u / (dU/dz)$  which roughly means that  $L_{MM} \approx z$  in the surface layer (if the approximation  $\sigma_u \approx u_* / \kappa$  is used), whereas our relation  $L_{MM} \approx 1.7\ell$  roughly means  $L_{MM} \approx 0.68z$ . The latter is also in accordance with*

*the work of Chougule et al. (2014) from measurements at Høvsøre and at Ryningsnäs.”*

First, this is only approached in the *neutral* surface layer (ASL). Secondly, for  $\sigma_u/u_* \approx 2.3$  (as shown in sections 2–3, and also found for the data sets in the neutral ASL), then  $L_{MM}|_{\text{inASL}} \approx 2.3z/\kappa \simeq 0.92z$  as given at the beginning of section 2.3.

Chougule *et al.* (2014, e.g. Fig. 5) actually shows agreement with  $L_{MM} \sim z$  in the ASL ( $z = 20\text{m}$ ) at Høvsøre (though their analysis is only for  $U$  between 7–8 m/s). At Ryningsnäs, when accounting for the displacement height ( $d \simeq 13\text{m}$ ) then their results are again consistent with the above, with  $L_{MM} \approx z - d$  or actually slightly larger (though affected by roughness-sublayer effects above the forest there).

*“3. So what is the reason for the differences between Peña et al. (2010)/Chougule et al. (2014) and your results? Could it be the way the velocity spectra was analyzed (you seem to extract the Mann parameters from each individual 10-min record whereas Peña et al. (2010)/Chougule et al. (2014) ensemble average spectra for different turbulence conditions)? What is the uncertainty of the fit when performed on each 10-min case?”*

As noted in my response to point 2 above, in the *neutral surface layer* there are not significant differences.

Overall, the increase of  $L_{MM}$  in unstable conditions is significantly larger than the decrease in stable conditions, as also implied e.g. in Sathe *et al.* (2012). The vertical range and extent to which  $\langle L_{MM} \rangle \sim z$  in all conditions depends on the (relative) widths of the stable- and unstable sides of the stability distribution  $P(1/L)$  as well as the distribution of ASL depth.

As for the uncertainty on spectrally-fit  $L_{MM}$ , this is beyond the scope of the current article—though I do note that the fit was improved markedly by rejecting  $\Gamma > 4.95$  (which corresponds to the fit using the highest  $\Gamma$  of the lookup-table of Mann-model outputs), and such rejection roughly appeared to eliminate potential bias in  $L_{MM}$ ; the latter is included as a footnote in section 3.2. Continuing work includes checking such fitting uncertainty/variability, as well as analysis per wind speed bin.

# From standard wind measurements to spectral characterization: turbulence length scale and distribution

Mark Kelly<sup>1</sup>

<sup>1</sup>Wind Energy Department, Risø Lab./Campus, Danish Technical University; Roskilde 4000, Denmark.

*Correspondence to:* Mark Kelly (MKEL@DTU.DK)

## Abstract.

In wind energy, the the effect of turbulence upon turbines is typically simulated using wind ‘input’ time-series based on turbulence spectra. The velocity components’ spectra are characterized by the amplitude of turbulent fluctuations, as well as the length scale corresponding to the dominant eddies. Following the IEC standard, turbine loads calculations commonly involve use of the Mann spectral-tensor model to generate timeseries of the turbulent three-dimensional velocity field. In practice, this spectral-tensor model is employed by adjusting its three parameters: the dominant turbulence length scale  $L_{MM}$  (peak length scale of an undistorted isotropic velocity spectrum), the rate of dissipation of turbulent kinetic energy  $\varepsilon$ , and the turbulent eddy-lifetime (anisotropy) parameter  $\Gamma$ . Deviation from ‘ideal’ neutral sheared turbulence—i.e. for non-zero heat flux and/or heights above the surface layer—is, in effect, captured by setting these parameters according to observations.

Previously, site-specific  $\{L_{MM}, \varepsilon, \Gamma\}$  were obtainable through fits to measured three-dimensional velocity component spectra recorded with sample rates resolving the inertial range of turbulence ( $\gtrsim 1$  Hz); however, this is not feasible in most industrial wind energy projects, which lack multi-dimensional sonic anemometers and employ loggers that record measurements averaged over intervals of minutes. Here a form is derived for the shear dependence implied by the eddy-lifetime prescription within the Mann spectral-tensor model, which leads to derivation of useful forms of the turbulence length scale. Subsequently it is shown how  $L_{MM}$  can be calculated from commonly-measured site-specific atmospheric parameters, namely mean wind shear ( $dU/dz$ ) and standard deviation of streamwise fluctuations ( $\sigma_u$ ). The derived  $L_{MM}$  can be obtained from standard (10-minute average) cup anemometer measurements, in contrast with an earlier form based on friction velocity.

The new form is tested across several different conditions and sites, and is found to be more robust and accurate than estimates relying on friction velocity observations. Assumptions behind the derivations are also tested, giving new insight into rapid-distortion theory and eddy-lifetime modelling—and application—within the atmospheric boundary layer. The work herein further shows that distributions of turbulence length scale, obtained using the new form with typical measurements, compare well with distributions  $P(L_{MM})$  obtained by fitting to spectra from research-grade sonic anemometer measurements for the various flow regimes and sites analyzed. The new form is thus motivated by and amenable to site-specific probabilistic loads characterization.



# 1 Introduction

Of the atmospheric parameters which are generally input into (or required by) wind turbine loads calculation codes, several stand out, due to their prominence in load contributions. ~~These are:~~ the ‘mean’ wind speed  $U$ , the standard deviation of streamwise turbulent velocity  $\sigma_u$ , the shear  $dU/dz$  or shear exponent  $\alpha$  ~~(calculated from wind speeds at multiple heights, e.g. Kelly et al. (2014a))~~, and the characteristic turbulence length scale  $L$  corresponding to the most energetic turbulent motions (e.g. Wyngaard, 2010). Dimitrov et al. (2015) explored the importance of shear ( $\alpha$ ); Dimitrov et al. (2017) found that both fatigue and extreme turbine loads can be sensitive to  $L$  in addition to the dominant influences of mean wind speed  $U$  and streamwise turbulence ‘strength’  $\sigma_u$ .<sup>1</sup> These are also consistent with the earlier finding of Sathe et al. (2013) that stability could affect fatigue loads through  $\alpha$  and  $\sigma_u$ .

Within the context of obtaining site-dependent statistics of the most ~~relevant crucial~~ load-driving parameters ~~from typical or standard~~  $(U, \sigma_u, \alpha, L)$  from conventional industrial wind measurements, we focus upon the relevant parameter which is this work focuses on the one parameter which has thus far been most difficult to measure: the ‘Mann-model length-scale’  $L_{MM}$  (Mann, 1994); i.e., the measure: the turbulence length scale  $L$ . The turbulence length scale, which corresponds to the ‘energy-containing sub-range’ of turbulence which contributes turbulent velocity fluctuations associated with the peak of the streamwise velocity spectrum, which contribute most to turbulent velocity fluctuations (and also turbine loads kinetic energy (and  $\sigma_u$ ))—and which can dominate the turbulence contribution to wind turbine loads. Measurements used in wind energy are usually stored as 10-minute statistics (average and standard deviation of wind speed and direction), so one cannot obtain turbulence spectra from them, nor can one calculate integral time or length scale from such observations.

~~Independent derivation of some~~ Because of its widespread use in the wind industry and its inclusion in the IEC 61400–1, Edition 3 (2005) standard on design requirements for wind turbines, here we consider the spectral turbulence model of Mann (1994), and  $L$  as prescribed for this model. Within the ‘Mann-model,’ which uses rapid-distortion theory (‘RDT’) to account for shear-induced distortion of isotropic turbulence Savill (1987); Savill (2000), there is also a prescription for the scale-dependent time over which turbulent eddies of a given size are distorted. This time-scale is key to proper representation of atmospheric turbulence and reproduction of component spectra via RDT. However, the eddy-lifetime relations has also been done concurrently by de Mare and Mann (2016), towards creation of ~~was not directly derived, but rather cleverly prescribed, by Mann (1994). Concurrent to and independent of the work herein, de Mare and Mann (2016) also derived some relations to create a model for time-varying eddy lifetime. The present article provides direct derivation of the eddy lifetime, which results in a relation between the three (spectral) parameters of the Mann model and measureable quantities. More importantly, the derivations here include connection of the turbulence length scale to routinely available quantities from typical 10-minute industrial wind records. The turbulence length scale is in fact that corresponding to the von Kármán (1948) spectral form, and thus the relation here is applicable to other turbulence models used in wind engineering, such as those relying on the Kaimal et al. (1972) spectrum.~~

---

<sup>1</sup>To a lesser extent there has also been found some sensitivity to the Mann-model anisotropy parameter  $\Gamma$ .

~~Dimitrov et al. (2017) found that both fatigue and extreme turbine loads can be sensitive to  $L_{MM}$  (as well as~~ After deriving the eddy lifetime and giving subsequent expressions for the turbulence length scale, this article proceeds to validation of the underlying assumptions. Constraints implied by fitting the Mann-model to measured spectra in non-neutral conditions, given eddy-lifetime and mixing-length relations, are also tested. This includes dependence of predicted velocity variance on model anisotropy parameter ( $\Gamma$ ), ~~in addition to~~ as well as implications in the ~~dominant influences of mean wind speed  $U$  and streamwise turbulence ‘strength’  $\sigma_u$ . This is also consistent with the earlier finding of Sathe et al. (2013), whom found that stability could affect fatigue loads~~ surface-layer and connection to previous findings in boundary-layer meteorology. Finally, the length-scale obtained from conventional 10-minute wind measurements via the new expression is compared to the length scale found from fits of Mann-model output to measured component spectra; this is done using data from multiple sites, representing several types of site conditions.

## 2 Theory

Relation of the turbulence length (spectral ‘peak’) scale to measureable statistics is possible through the eddy-lifetime form of Mann (1994), where the latter is defined in terms of the isotropic von Kármán spectrum that is distorted using RDT.

### 2.1 Eddy lifetime

A number of forms exist to estimate eddy lifetime  $\tau_e$ , though these can be generally expressed as the ratio of a length scale (taken as the reciprocal of wavenumber,  $k^{-1}$ ) to a velocity scale which follows from some integrated form of the (scalar) kinetic energy spectrum  $E(k)$ :

$$\tau_e \sim k^{-p-1} \left[ \int_k^\infty \kappa^{-2p} E(\kappa) d\kappa \right]^{-1/2}, \quad (1)$$

where the characteristic velocity scale can be generically described by

$$k^p \left[ \int_k^\infty \kappa^{-2p} E(\kappa) d\kappa \right]^{1/2}.$$

Comparing to the ‘coherence-destroying diffusion time’ of Comte-Bellot and Corrsin (1971) and to the reciprocal of eddy-damping rates from Lesieur (1990), for use with rapid-distortion theory Mann (1994) chose an eddy lifetime that depends on eddy size (wavenumber) according to

$$\tau_M \propto k^{-1} \left[ \int_k^\infty E(\kappa) d\kappa \right]^{-1/2}; \quad (2)$$

i.e., equivalent to  $p = 0$  in terms of (1). The choice (2) for eddy lifetime was found to behave more reasonably than both the Comte-Bellot and Corrsin (1971) ‘diffusion time’ (where  $p = 1$ )<sup>2</sup>, as well as the timescale  $[k^3 E(k)]^{-1/2}$  (which in the inertial

<sup>2</sup> The Mann (1994) expression is also equivalent (or at least proportional) to the ‘convection time’ of Comte-Bellot and Corrsin (1971).

range is equivalent to  $p = -1$ )<sup>3</sup> implicit in eddy-damped quasi-normal Markovian [EDQNM] models (Andre and Lesieur, 1977; Lesieur, 1990); both of the latter lifetime models do not (reliably) integrate to give finite  $\sigma_u^2$ .

Mann (1994) re-writes  $\tau_M$  as

$$\tau_M(k) = \frac{\Gamma}{dU/dz} \frac{(kL_{MM})^{-2/3}}{\sqrt{{}_2F_1\left(\frac{1}{3}, \frac{17}{6}, \frac{4}{3}; \frac{-1}{(kL_{MM})^2}\right)}}, \quad (3)$$

- 5 where  ${}_2F_1$  is Gauss' hypergeometric function (Abramowitz and Stegun, 1972)<sup>4</sup> and  $L_{MM}$  is the turbulence length scale associated with the peak of the turbulent kinetic energy spectrum  $E(k)$  as in (2). The eddy lifetime definition (3) is used in practical implementation of the spectral tensor model (e.g. Mann, 2000), and it notably defines a parameter of this model: the eddy lifetime scaling parameter factor  $\Gamma$ , also known as the anisotropy factor. The Mann (1994) spectral-tensor model employs rapid distortion theory ('RDT') with an-, whereby the shear  $dU/dz$  distorts turbulence from an isotropic state, based  
 10 on an initial turbulent kinetic energy spectrum of the isotropic von Kármán form von Kármán form

$$E_{vK}(k) = \alpha \varepsilon^{2/3} L_{MM}^{5/3} \frac{(kL_{MM})^4}{[1 + (kL_{MM})^2]^{17/6}}; \quad (4)$$

with where  $\alpha = 1.7$  (von Kármán, 1948). This in effect defines the length scale  $L_{MM}$  through the peak of the initial spectrum.<sup>5</sup>

Using (4) in the proportionality expression (2) produces

$$\tau_{M|E \rightarrow E_{vK}} = \frac{c_\tau k^{-2/3}}{\sqrt{\frac{3}{2} \alpha \varepsilon^{2/3} {}_2F_1\left(\frac{1}{3}, \frac{17}{6}, \frac{4}{3}; \frac{-1}{(kL_{MM})^2}\right)}}, \quad (5)$$

- 15 where we have introduced the coefficient proportionality constant  $c_\tau$  to equation write the result of integrating the proportionality relation (2) with (3) as an equation. Then we have an expression relating the Mann-model parameters to the shear  $dU/dz$ :

$$\Gamma = \frac{c_\tau}{\sqrt{3\alpha/2}} \frac{dU}{dz} \frac{L_{MM}^{2/3} \varepsilon^{-1/3}}{\varepsilon}.$$

Now  $\tau_M$  can be seen to depend upon  $k$ ,  $L_{MM}$ , and  $\varepsilon$ . The eddy-lifetime can be reduced and clarified via  ${}_2F_1\left\{\frac{1}{3}, \frac{17}{6}; \frac{4}{3}; (-kL_{MM})^{-2}\right\} \simeq [1 + 3.07(kL_{MM})^{-2}]^{-1/3}$  to give the more understandable transparent von Kármán-like form<sup>6</sup>

$$20 \quad \tau_M(k; L_{MM}, \varepsilon) \simeq \frac{0.82c_\tau}{\sqrt{\alpha \varepsilon^{2/3}}} k^{-2/3} \left[1 + \frac{3.07}{(kL_{MM})^2}\right]^{1/6}. \quad (6)$$

<sup>3</sup> The reciprocal of eddy-damping rate,  $[k^3 E(k)]^{-1/2}$ , is equal in the inertial range to (1) with  $p = -1$  since  $E(k) \rightarrow \kappa^{-5/3}$  there. This expression is also similar to the 'rotation time' or 'strain time' given by Comte-Bellot and Corrsin (1971), but it should be noted that such expressions integrate from 0 to  $k$ , i.e. over eddies larger than  $1/k$ .

<sup>4</sup> The hypergeometric function  ${}_2F_1\left[\frac{1}{3}, \frac{17}{6}; \frac{4}{3}; -(kL_{MM})^{-2}\right]$  approaches 1 for  $kL_{MM} \gg 1$  (the inertial range), and simplifies to  $a_{HG}(kL_{MM})^{2/3}$  for  $kL_{MM} \ll 1$ , where  $a_{HG} \equiv (3\sqrt{\pi}/4)f_\Gamma(4/3)/f_\Gamma(17/6) \simeq 0.69$  and  $f_\Gamma(x)$  is the Euler-gamma function.

<sup>5</sup> The peak of the von Kármán isotropic TKE spectrum  $E_{vK}(k)$  occurs at  $kL_{MM} = \sqrt{12/5}$ , i.e.  $L_{MM} \simeq 1.55/k_{peak}$ .

<sup>6</sup> Note  $\sqrt{2/3} \simeq 0.82$ , and  $3.07 = a_{HG}^{-3}$ ; c.f. footnote 4. In (6),  $\alpha \varepsilon^{2/3}$  is kept together for comparison with (4), and because  $\alpha \varepsilon^{2/3}$  is commonly used as an input to the spectral-tensor model instead of  $\varepsilon$  (e.g. Mann et al., 2002; IEC 61400-1, Edition 3, 2005).

Since (3) and (5) are equal, we have an expression relating the Mann-model parameters to the shear  $dU/dz$ :

$$\Gamma = \frac{c_\tau}{\sqrt{3\alpha/2}} \frac{dU}{dz} L_{\text{MM}}^{2/3} \varepsilon^{-1/3}. \quad (7)$$

The expression (7) can be made yet more useful to relate the turbulent length scale to measureable parameters, as shown in section 2.2.

### 5 2.1.1 Eddy lifetime and equilibrium

The parameters  $\{\varepsilon, \Gamma, L_{\text{MM}}\}$  are site-dependent, and in practice have been obtained from measurements through fits of the model output to observed spectra (Mann, 2000), relying on (at least three of)  $F_{11}$ ,  $F_{13}$ ,  $F_{33}$ , and  $F_{22}$  (e.g. Sathe et al., 2013; Dimitrov et al., 2017). The model starts with an (undistorted) isotropic incompressible turbulence spectral tensor

$$\Phi_{ij}(\mathbf{k}) \Big|_0 = \frac{\delta_{ij}k^2 - k_i k_j}{4\pi k^4} E(k) \quad (8)$$

10 where  $E(k)$  is taken to be  $E_{\text{vK}}(k)$  following shown in (4), then the  $\Phi_{ij}$  are distorted—i.e. the rapid-distortion equations are solved—per (three-dimensional) wavenumber over a time  $\tau_M(k)$  via rapid-distortion theory [‘RDT’].

The rapid-distortion equations discussed here do not explicitly solve for production of normal stresses (which sum to twice the turbulent kinetic energy) nor shear stress, though they do include (Fourier-transformed) terms for perturbing isotropic terms that perturb the stresses<sup>7</sup> to account for the anisotropic (anisotropic) effect of a constant shear  $dU/dz$ ; however, RDT. Further, the RDT discussed here does not include dissipation (e.g. Pope (2000)). Instead (Mann, 1994; Mann, 2000); instead, in the spectral-tensor model the dissipation rate of turbulent kinetic energy  $\varepsilon$  is a parameter giving the amplitude of the undistorted (initial) spectrum via (4); ~~ε can also be~~ In practice  $\varepsilon$  is obtained via fits of precalculated pre-calculated Mann-model output to measured (distorted) spectra, spectra, so  $\varepsilon$  effectively in effect gives the inertial-range amplitudes of the distorted velocity component spectra, which have been distorted for a time  $\tau_M(k)$ . The From (3) one sees that the parameter  $\Gamma$  serves as a factor that determines the amount of distortion and associated anisotropy—and thus anisotropy: increasing  $\Gamma$  corresponds to longer distortion time  $\tau_M$  and thus more anisotropy, with  $\Gamma = 0$  corresponding to isotropy (zero distortion of the initial isotropic  $\Phi_{ij}$ ). The separation between the peaks of the different component spectra (the  $ww$ -spectrum peak increases with  $\Gamma$ ; the spectral peak of  $F_{33}$  is at higher wavenumbers than  $vv$ -peak (smaller scales) than the  $F_{22}$  peak, which is at higher  $k_1$  than the  $uu$  spectral peak); increasing  $\Gamma$  (Mann, 1994) corresponds to more anisotropy. wavenumbers than the peak of  $F_{11}$  (Mann, 1994). Thus a stationary equilibrium result is achieved via the eddy-lifetime prescription together with rapid-distortion of an isotropic spectrum—with the isotropic spectral tensor—with  $\tau_M$  and (initial) inertial-range amplitudes and also  $\tau_M$  both depending on  $\varepsilon$  (via eqns. 3 and 7)—whereby (3–4, 7), whereby shear-production of TKE is in effect balanced by dissipation. The I.e., the resultant shear stress  $\langle uv \rangle$  (expressible now in terms of  $\varepsilon$ ) can be multiplied by  $2\partial U/\partial z$  to give the implied production rate

<sup>7</sup>Assuming a constant mean shear  $dU/dz$ , the spectral-tensor model solves (Fourier-transformed versions of ) rapid-distortion equations for streamwise normal stress  $\langle u_1 u_1 \rangle$  and shear stress  $\langle u_1 u_3 \rangle$ ; multiplying these by  $dU/dz$  one obtains the corresponding production rates:  $P_{11} = -2\langle u_1 u_3 \rangle dU/dz$  and  $P_{13} = -\langle u_3 u_3 \rangle dU/dz$  (Pope, 2000, Ch.11).

of  $\langle uu \rangle$ , which with  $vv$  and  $ww$  (through  $\Gamma$ ) gives the implied TKE production rate, amounting to  $P = \varepsilon$ ; such an equilibrium, enforced by  $\tau_M$ , can also be inferred from de Mare and Mann (2016).

## 2.2 Characteristic length scale

Noting that the spectrum of a variable integrates to the variance of said variable, then invoking (8) with the isotropic von Kármán form (4) for  $E(k)$  and exploiting  $F_{11}(k_1) = \iint \Phi_{11} dk_2 dk_3$ , one obtains the isotropic streamwise turbulence variance

$$\begin{aligned} \sigma_{\text{iso}}^2 &= 2 \int_0^{\infty} \frac{9}{55} \alpha \varepsilon^{2/3} L_{\text{MM}}^{5/3} [1 + (k_1 L_{\text{MM}})^2]^{-5/6} dk_1 \\ &= 0.69 \alpha \varepsilon^{2/3} L_{\text{MM}}^{2/3} \end{aligned} \quad (9)$$

which is the undistorted streamwise variance. The factor 0.69 is the numerical value of  $\frac{9}{55} \sqrt{\pi} f_{\Gamma}(\frac{1}{3}) / f_{\Gamma}(\frac{5}{6})$  and  $f_{\Gamma}(x)$  is the Euler gamma function (Abramowitz and Stegun, 1972, see also footnote 4 above). Then using (9) in (7) we get a relation for the isotropic (undistorted) turbulence length scale implied by the lifetime-model (3),

$$L_{\text{MM}} \simeq \left( \frac{1.5\Gamma}{c_{\tau}} \right) \frac{\sigma_{\text{iso}}}{dU/dz}, \quad (10)$$

where the leading term in parenthesis is expected to be of order 1.

### 2.2.1 Relation to observations

Peña et al. (2010) suggested that the Mann-model length scale is proportional to the classic mixing length  $\ell_* \equiv u_*/(dU/dz)$  multiplied by an empirical constant, i.e.

$$L_{\text{MM}} = c_m \ell_* = \frac{c_m u_{*,\text{obs}}}{dU/dz} \quad (11)$$

where they assign  $c_m = 1.7$ . However, we find from observations that on average  $c_m \approx 2.3$  over flat land, i.e.  $\langle L_{\text{MM}}/\ell_* \rangle = 2.3$  (see next section). Combining (10)–(11) one sees that  $c_{\tau}$  decreases with the relative magnitude of measured shear stress (as  $\sigma_{\text{iso}}/u_{*,\text{obs}}$ ); this is also expressed usefully through the measured ratio of streamwise fluctuation amplitude to friction velocity:

$$c_{\tau} \simeq \frac{1.5\Gamma}{c_m} \frac{\sigma_{\text{iso}}}{u_{*,\text{obs}}} = \frac{1.5\Gamma}{\sigma_{u,\text{obs}}/\sigma_{\text{iso}}} \left( \frac{\sigma_{u,\text{obs}}/u_{*,\text{obs}}}{c_m} \right). \quad (12)$$

From the above and (10) one subsequently then finds

$$L_{\text{MM}} \simeq \frac{\sigma_{u,\text{obs}}}{dU/dz} \left( \frac{c_m}{\sigma_{u,\text{obs}}/u_{*,\text{obs}}} \right). \quad (13)$$

For constant  $(\sigma_{u,\text{obs}}/u_{*,\text{obs}})$ , (13) implies that the turbulence scale  $L_{\text{MM}}$  can be expressed *independently* of  $\Gamma$ , given  $\sigma_{u,\text{obs}}$  and  $dU/dz$ .

Caughey et al. (1979) reported the mean profile of  $\sigma_u^2(z)$  from the seminal ‘Kansas experiment’, showing that  $(\sigma_u/u_*)^2 \approx 5-6$  in the homogeneous atmospheric surface layer (their Fig. 5). The corresponding value of  $(\sigma_u/u_*)_0$  is approximately 2.3; thus, if  $c_m \approx 2.3$  as well, then (12) reduces to

$$c_\tau \approx \frac{1.5\Gamma}{\sigma_{u,\text{obs}}/\sigma_{\text{iso}}}. \quad (14)$$

- 5 Given the definition of  $c_\tau$  through (7),  $c_\tau$  is a constant; since (9) shows  $\sigma_{\text{iso}}$  is independent of  $\Gamma$ , then  $\sigma_{u,\text{obs}} \propto \Gamma$ . Consistent with this argument, (13) reduces to

$$L_{\text{MM}} \approx \frac{\sigma_{u,\text{obs}}}{dU/dz} \quad (15)$$

- which is also evident inserting (14) into (10). Using (15),  $L_{\text{MM}}$  can simply be diagnosed from typical measurements, e.g. 10-minute average cup-anemometer output, at two (or more) heights. The length  $L_{\text{MM}}$  can also be cast in terms of variables commonly used in wind engineering, notably the turbulence intensity  $I_u$  and shear exponent  $\alpha$ . Invoking  $dU/dz = \alpha U/z$  (Kelly et al., 2014a) and defining  $I_{\text{obs}} \equiv \sigma_{u,\text{obs}}/U$ , then (15) becomes  ~~$L_{\text{MM}} \approx z I_{\text{obs}}/\alpha$~~

$$L_{\text{MM}} \approx z \frac{I_{\text{obs}}}{\alpha}. \quad (16)$$

### 2.2.2 Modelled spectra: covariances, anisotropy and $\Gamma$

- The spectral Mann-model (‘MM’) distorts the isotropic von Kármán spectral tensor ( $\Phi_{ij}(\mathbf{k})$ , eq. 4), per wavenumber via rapid-  
15 distortion theory over the wavenumber-dependent eddy-lifetime  $\tau_M$ , such that the component spectra become anisotropic at wavenumbers outside (lower than) the inertial range; the degree of distortion—and thus anisotropy—are consequently represented by the eddy-lifetime parameter  $\Gamma$ . Above we showed via mixing-length arguments that  $L_{\text{MM}}$  is independent of  $\Gamma$ , resulting in (15). Possible  $\Gamma$ -dependences can also be examined by considering the shear stress

$$\langle ww \rangle_{\text{MM}} = -u_{*,\text{MM}}^2 = 2 \int_0^\infty F_{13}(k_1) dk_1 \quad (17)$$

- 20 obtained from the modelled spectral tensor component  $F_{13}(k_1) = \iint \Phi_{13} dk_2 dk_3$ , which is expected to be a function of  $\Gamma$ . Indeed Mann (1994, Figure 4) shows this to be the case, with modeled stress  $\langle ww \rangle_{\text{MM}}/\sigma_{\text{iso}}^2$  varying almost linearly between 0 and  $-1$  for  $0 < \Gamma < 5$ ; then  $u_{*,\text{MM}}^2/\sigma_{\text{iso}}^2 \approx \Gamma/5$ . Subsequently from (12) one has

$$c_\tau \approx \frac{1.5\sqrt{5}\Gamma}{c_m} \frac{u_{*,\text{MM}}}{u_{*,\text{obs}}} \approx \frac{0.64\Gamma}{u_{*,\text{obs}}/\sigma_{\text{iso}}} \quad (18)$$

for  $c_m \approx 2.3$ , in analogy with (14); thus we expect  $u_{*,\text{obs}} \propto \Gamma$ , similar to the expected behavior of  $\sigma_{u,\text{obs}} \propto \Gamma$  following (14).

- 25 In addition to the approximate expression (18), which is based on the simplified relation  $u_{*,\text{MM}}^2/\sigma_{\text{iso}}^2 \approx \Gamma/5$ , it is possible to derive an exact relation based on the the Mann-model shear stress (17); but this is cumbersome and analytically intractable. Though de Mare and Mann (2016) derived implicit expressions toward relating  $\{\Gamma, dU/dz, L_{\text{MM}}\}$  to the eddy lifetime and integral of the modelled stress spectrum (17), these must be evaluated numerically or graphically. An explicit expression

corresponding to  $c_m^{-1} = \ell_*/L_{\text{MM}}$  (like eqn. 11 here) was derived by de Mare and Mann (2016), but it depends on numerically integrating the stress spectrum.

As spectra fitted to Mann-model outputs correspond to distorted *anisotropic* turbulence, and noting the  $\Gamma$ -dependence of  $u_{*,\text{MM}}$  discussed above, we expect  $\sigma_{u,\text{MM}}$  to also depend on  $\Gamma$ . From Figure 4 of Mann (1994) we find  $\sigma_{u,\text{MM}}^2/\sigma_{\text{iso}}^2 \simeq (1 + 0.14\Gamma^2)$ , which for  $\Gamma \gtrsim 2$ , the range corresponding to ABL observations (e.g. Sathe et al., 2013), becomes roughly  $\sigma_{u,\text{MM}} \approx \sigma_{\text{iso}}(0.61 + 0.3\Gamma)$ .

### 2.3 Ideal, neutral surface-layer implications

Within the atmospheric surface-layer (‘ASL’), in the homogeneous stationary (ideal) limit under neutral conditions,  $dU/dz \rightarrow u_*/(\kappa z)$  so that (11) reduces to  $L_{\text{MM}} \rightarrow c_m \kappa z \approx 0.92z$ . Similarly, in this ‘log-law regime’  $\varepsilon_{\text{ASL,N}} = u_*^3/(\kappa z)$ , so that (7) becomes  $\Gamma_{\text{ASL,N}} = c_\tau (3\alpha/2)^{-1/2} (L_{\text{MM}}/\kappa z)^{2/3}$  or equivalently  $L_{\text{MM}}|_{\text{ASL,N}} = (3\alpha/2)^{3/4} \kappa z [\Gamma/c_\tau]^{3/2}$  which via (12) can be written

$$L_{\text{MM}}|_{\text{ASL,N}} = \left(\frac{3\alpha}{2}\right)^{3/4} \kappa z \left[ \frac{c_m u_{*,\text{obs}}}{1.5\sigma_{\text{iso}}} \right]^{3/2} \simeq 1.1\kappa z \left[ \frac{c_m}{\sigma_{u,\text{obs}}/u_{*,\text{obs}}} \frac{\sigma_{u,\text{obs}}}{\sigma_{\text{iso}}} \right]^{3/2} \quad (19)$$

Thus for  $c_m = \sigma_{u,\text{obs}}/u_{*,\text{obs}}$ , we see that the Mann (1994) eddy-lifetime formulation (3) implies  $L_{\text{MM}} \rightarrow 1.1\kappa z (\sigma_{u,\text{obs}}/\sigma_{\text{iso}})^{3/2}$  in the neutral ASL. Meanwhile, as noted just above, the mixing-length form (11) implies  $L_{\text{MM}} \rightarrow c_m \kappa z$ ; this is consistent with (19) under the condition that  $(\sigma_{u,\text{obs}}/\sigma_{\text{iso}}) \simeq (c_m/1.1)^{2/3}$  or roughly  $\sigma_{u,\text{obs}} \approx 1.6\sigma_{\text{iso}}$  for  $c_m \simeq 2.3$ .

## 3 Observations and results

Since the choice of eddy lifetime form (3) leads to a shear-dependent relation (7) between the spectral-tensor model parameters, one obtains (10) for the undistorted (isotropic) length scale, with  $L_{\text{MM}} \propto \sigma_{\text{iso}} (dU/dz)^{-1}$ ; further invoking a mixing-length argument then leads to a relation (15) for  $L_{\text{MM}}$  in terms of quantities that are directly measureable via standard wind-industry (one-dimensional cup) anemometers. Here we test (15) as well the assumptions leading to it, through measured wind speed, shear, and turbulent velocity component spectra. We also find a form for the distribution of  $L_{\text{MM}}$  over all conditions—as would be needed in practice to represent the turbulence length scales of flows experienced by wind turbines at a given site.

~~The spectra~~ For the assumption-testing in this section, the spectra used are measured via three-dimensional sonic anemometers on the primary meteorological mast located at the Danish National Test Site for Large Wind Turbines (Høvsøre), 1.75 km from the western coast of Denmark (Mann et al., 2005; Peña et al., 2016). The anemometers give 20 Hz samples of all three velocity components and temperature<sup>8</sup> at heights of 10, 20, 40, 60, 80, and 100 m. This allows calculation of mean speeds, directions, and vertical shear of mean speed over individual 10-minute records; in particular we focus on heights of  $z=20$  m and  $z=80$  m, as we are able to calculate shear at (across) these heights using the measurements at 10, 40, 60, and 100 m, while also using the measured wind speed components and subsequent spectra at  $z = \{20, 80\}$  m. The parameters  $\{L_{\text{MM}}, \Gamma, \epsilon\}$  are obtained via fits of precalculated Mann-model spectra to the measured velocity-component and stress spectra  $F_{11}(f)$ ,  $F_{22}(f)$ ,

<sup>8</sup>The sonic anemometers actually give a temperature very close to the virtual temperature, i.e. the temperature including buoyant effects of water vapor.

$F_{33}(f)$ , and  $F_{13}(f)$ ; this is done via Taylor's hypothesis ( $k_1 = 2\pi f/U$ ) ~~and chi-squared along with combined least-squares~~ fits (Mann, 1994; Chougule et al., 2017).

### 3.1 Testing of assumptions and predicted constraints

The implications of (12–15) included the independence of  $L_{MM}$  and  $c_\tau$  from  $\Gamma$ , as well as e.g. the expected dependence  $\sigma_{u,obs} \propto \Gamma\sigma_{iso}$ . Indeed we find that  $L_{MM}$  is independent of  $\Gamma$ , with no significant statistical correlation:  $\langle L_{MM}\Gamma \rangle / \sqrt{\langle L_{MM}^2 \rangle \langle \Gamma^2 \rangle} < 0.15$  for land or sea sectors at any given height. We also confirm that  $\sigma_{u,obs} \propto \Gamma\sigma_{iso}$ , which is demonstrated by Figures 1–2. The first figure displays the joint probability density  $P(\sigma_{u,obs}, \sigma_{iso})$ , where  $\sigma_{u,obs}$  is the streamwise turbulent variance measured in 10-minute intervals, and  $\sigma_{iso}$  is calculated using (9) with  $L_{MM}$  and  $\epsilon$  from spectral fits corresponding to the same intervals. One can see from [Fig. Figure 1](#) that  $\sigma_{u,obs}$  generally follows  $\sigma_{iso}$ , and we find  $\frac{\sigma_{u,obs}^2}{\sigma_{iso}^2} \approx 3 \frac{\sigma_{u,obs}}{\sigma_{iso}} \approx 5/3$ ; that is  $\sigma_{u,obs}/\sigma_{iso} \approx 1.7$ . Such evidence corresponds closely to the predicted constraint following (19) that  $\sigma_{u,obs}/\sigma_{iso}$  should have a value of roughly 1.6 in the neutral surface layer; this is reasonable in the mean, since conditions on average are essentially neutral due to the shape of the stability distribution at Høvsøre (Kelly and Gryning, 2010). Figure 2 further shows that  $\sigma_{u,obs}/\sigma_{iso} \propto \Gamma$ , consistent with  $c_\tau$  being a constant independent of  $\Gamma$  following (14). The slope of the line in Fig. 2 also corresponds to the ~~behavior implied by the~~ approximate Mann-model behavior  $\sigma_{u,MM} \approx \sigma_{iso}(0.61 + 0.3\Gamma)$  for  $\Gamma \gtrsim 2$ , outlined at the end of section 2.2.2 above.

~~Considering only wind speeds above  $7 \text{ m s}^{-1}$  (i.e. ignoring low speeds that have little impact on turbine loads),~~ [Considering wind speeds in the typical turbine operating range of  \$4\text{--}25 \text{ m s}^{-1}\$](#) , the Høvsøre data also confirm that  $\langle \sigma_u/u_* \rangle_{obs} \approx 2.3$ , consistent with the findings of Caughey et al. (1979). Further, ~~for these significant wind speeds,~~ the data also show that  $\langle c_m \rangle \approx 2.3$ , so that (13) reduces approximately to (15). ~~Figures 1–2 were made considering  $U > 7 \text{ m s}^{-1}$ , though they are essentially the same when including speeds down to~~ [It is also found that the same approximate trends are seen when considering only  \$4U > 7 \text{ m s}^{-1}\$  \(with slightly more scatter \(not shown\), but with slightly less scatter \(narrower joint distributions\) away from the main trends shown\).](#) ~~For the remainder of the figures, we continue to consider  $U > 7 \text{ m s}^{-1}$ .~~ [predicted  \$\sigma\_{u,obs}/\sigma\_{iso}\$  behaviors shown in Figures 1–2 \(dashed/dotted lines\) and discussed above.](#)

The data also show that  $\sigma_u/u_*$  is not correlated with  $L_{MM}$ , whether we include all speeds, or limit the wind speed range to  $7\text{--}25 \text{ m s}^{-1}$  or  $4\text{--}25 \text{ m s}^{-1}$ . Thus this ratio can be treated as a constant in (13) for a given height (or throughout the surface layer), using (13) over a range of wind speeds.

### 3.2 Turbulence length-scale distributions $P(L_{MM})$

The efficacy of using (15) to estimate the spectral length scale  $L_{MM}$  can be seen by considering Figure 3. The figure displays the joint-distribution of turbulence length scale at a height of  $z = 80 \text{ m}$ , i.e.  $P(L_{MM,obs}, \sigma_{u,obs} | dU/dz |^{-1})$ ; this is obtained through (15) from 10-minute measurements and via fitting observed spectra. Fig. 3 is usefully interpreted as the probability-weighted performance of (15) for predicting  $L_{MM}$  (from  $\sigma_{u,obs}$  measured at  $z = 80 \text{ m}$  and the shear  $dU/dz$  observed over  $z = 60\text{--}100 \text{ m}$ ), versus the  $L_{MM}$  obtained from fits of the spectral-tensor model to corresponding 10-minute spectra. One sees



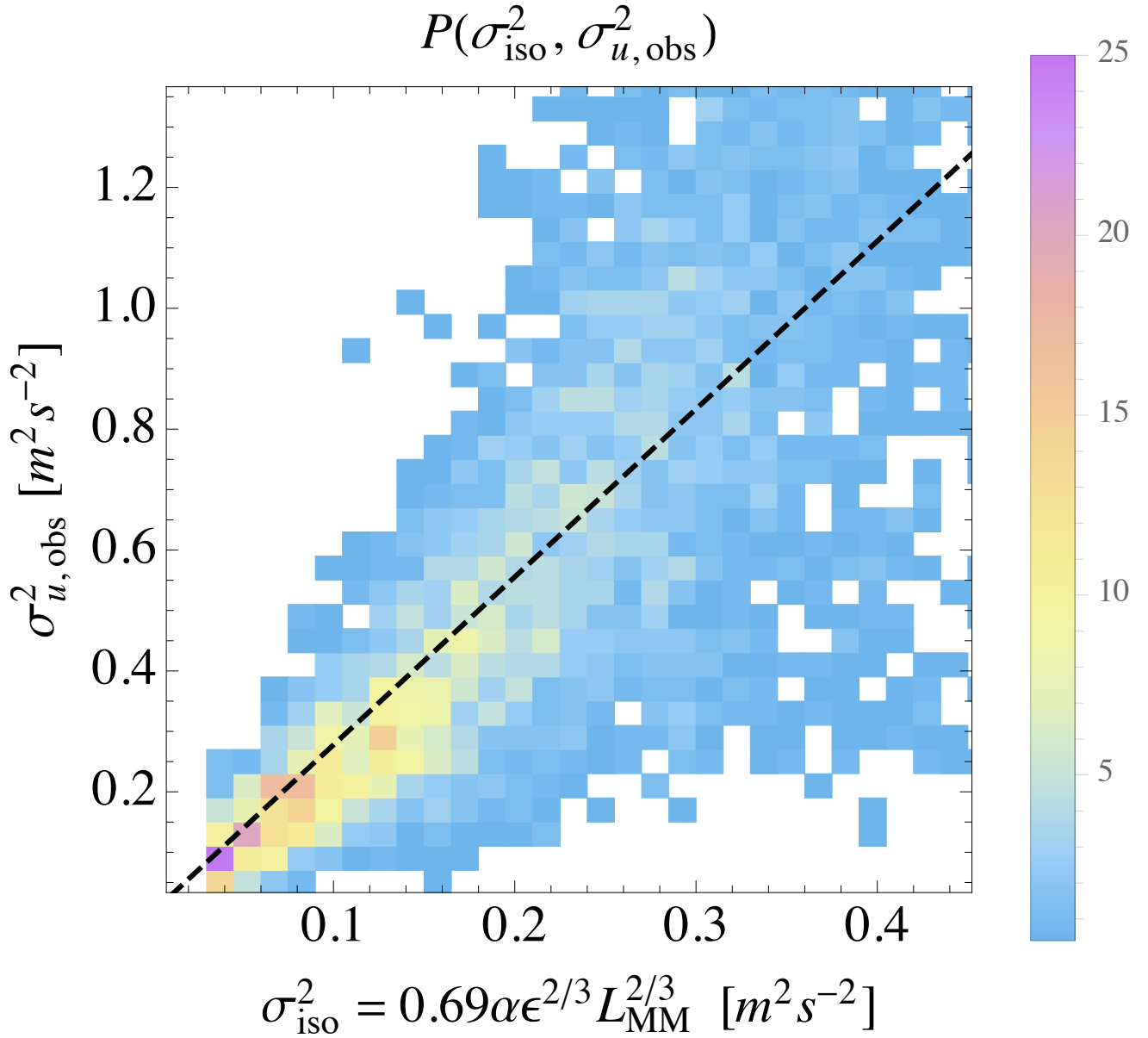


**Figure 1.** Joint distribution of isotropic (un-distorted) variance  $\sigma_{\text{iso}}^2(\epsilon, L_{\text{MM}})$  obtained from fits to measured spectra and observed stream-wise variance  $\sigma_{u, \text{obs}}$ , from height  $z=80$  m over homogeneous land sectors at Høvsøre; dashed line indicates a slope of 3, corresponds to  $\sigma_{u, \text{obs}}/\sigma_{\text{iso}} \approx 5/3$ .

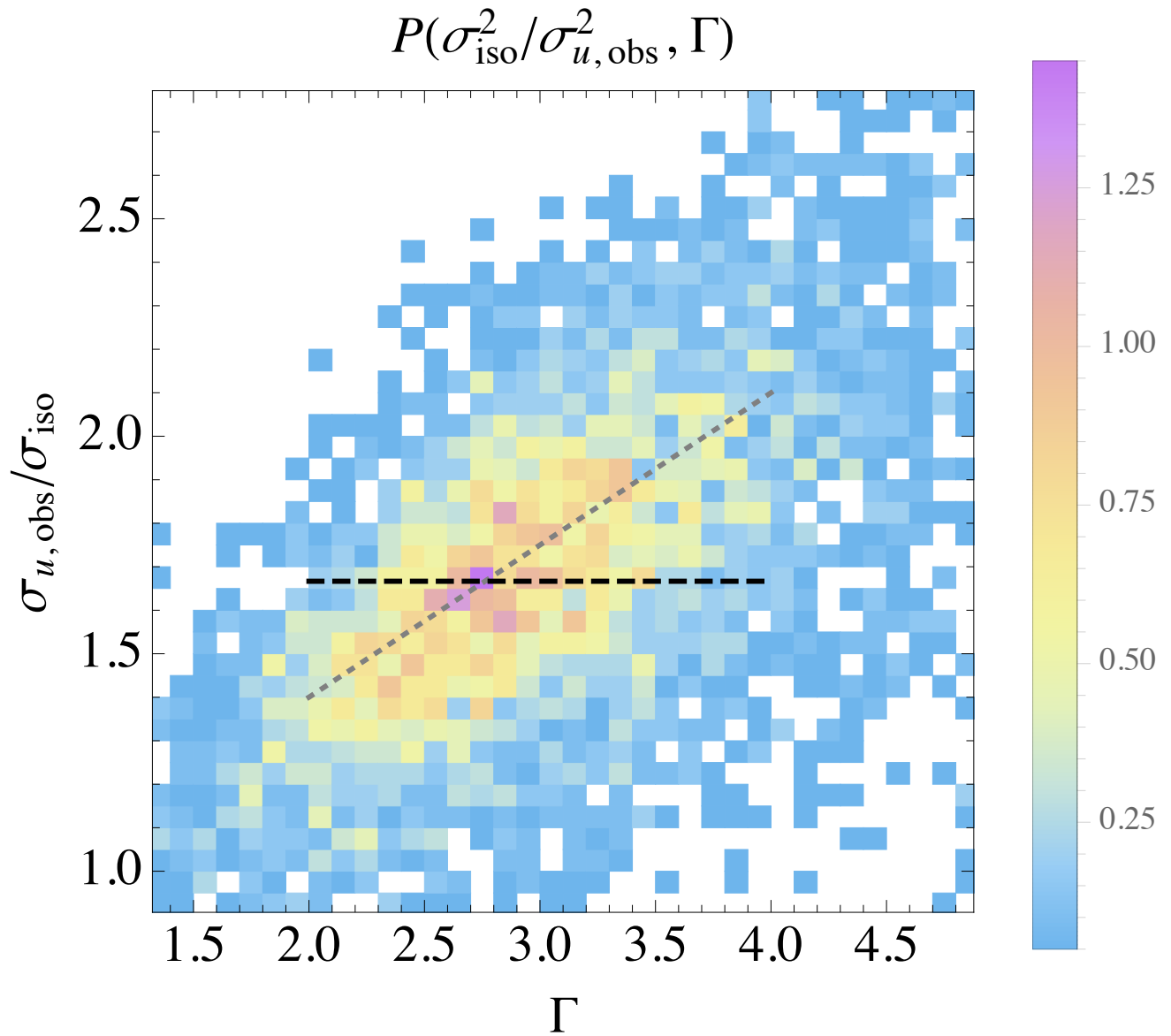


**Figure 2.** Ratio of observed streamwise to isotropic fluctuation magnitude, versus  $\Gamma$  obtained from spectral fits, plotted as joint-PDF  $P(\Gamma, \sigma_{u,\text{obs}}/\sigma_{\text{iso}})$ . Dashed (horizontal) line shows  $\sigma_{u,\text{obs}}/\sigma_{\text{iso}} = \sqrt{3} \sigma_{u,\text{obs}}/\sigma_{\text{iso}} = \sqrt{5/3}$  corresponding to slope of dashed line in Fig. 1; dotted line shows the mean linear  $\Gamma$ -dependence of  $\sigma_{u,\text{obs}}/\sigma_{\text{iso}}$ .

a 1:1 relationship, particularly for the most commonly-found values of the length scale; these  $L_{MM}$  range from  $\sim 15\text{--}50\text{ m}$ .<sup>9</sup> Compared to the scales calculated from observed spectra, there is some mis-prediction of  $L_{MM}$  calculated by (15), but it is relatively rare; this is shown by the low probabilities in Fig. 3 away from the well-predicted most commonly-occurring  $L_{MM}$ .

To demonstrate the statistical character of (15), as well as its potential for probabilistic use (e.g. as input to probabilistic loads calculations), Figure 4 shows the probability density  $P(L_{MM})$ . As in Fig. 3,  $L_{MM}$  is again calculated from fits to 10-minute spectra and also estimated by  $\sigma_{u,\text{obs}}/(dU/dz)$ , i.e. Eq. 15. Additionally Fig. 4 displays  $P(L_{MM})$  for  $L_{MM}$  calculated through (11), i.e.  $c_m u_*/(dU/dz)$ ; this is done both using the value of  $c_m = 1.7$  reported by Peña et al. (2010), as well as using the approximate mean of 2.3 found to be consistent with measurements and theory in sections 3.1 and 2.2 above. From Fig. 4 one sees that for values of turbulent peak scale greater than the mode ( $\sim 20\text{ m}$ ) up to roughly 150 m, there is a match between the distribution of the diagnosed  $L_{MM}$  and distributions of length scale estimated from the forms (15) based on  $\sigma_{u,\text{obs}}$  and (11) based on  $u_*$  with  $c_m = 2.3$ ; these are roughly equivalent for this case over relatively simple homogeneous terrain. It is found that the Peña et al. (2010) value of  $c_m = 1.7$  leads to overprediction of  $L_{MM}$  by a factor of 2 or more at scales smaller than 10 m, and underprediction by 50% or more at scales larger than 50 m. The  $u_*$ -based form (11) using  $c_m = 2.3$  matches the spectrally-fit diagnosed distribution  $P(L_{MM})$  slightly better than the  $\sigma_u$ -based form (15), with predicted peak (mode) values of  $L_{MM}$  being about 3–4 m smaller than the diagnosed peak- $L_{MM}$ .

For the homogeneous land case in Fig. 4 the PDF of  $2.3u_{*,\text{obs}}/(dU/dz)$  matches  $P(L_{MM})$  observed from the spectral fits to within 10%, over the range  $10\text{ m} \lesssim L_{MM} \lesssim 75\text{ m}$ , and the PDF of  $\sigma_{u,\text{obs}}/(dU/dz)$  also matches within 10% over the range  $15\text{ m} \lesssim L_{MM} \lesssim 50\text{ m}$ . This is consistent with the darkly-colored 1:1 patch evident in Fig. 3, and also shows that eqn. 15 (and also eqn. 11 with  $c_m = 2.3$ ) is sufficient for probabilistic wind loads simulations, for two reasons. First, the well-matched range of scales corresponds to the most commonly found  $L_{MM}$ . Secondly, although scales smaller than  $\sim 15\text{ m}$  are not rare (with an occurrence of roughly 1 in 6), they will have a diminishing effect on turbine loads. More specifically,  $L_{MM}$  is more than 70% likely to fall in the 15–75 m range, i.e.  $P(15\text{ m} < L_{MM} < 75\text{ m}) > 0.7$ , and  $L_{MM}$  has more than 86% likelihood of occurrence between 0 and 75 m, for this homogeneous land case at  $z = 80\text{ m}$ . The relatively common shorter scales correspond to weaker turbulent fluctuations (thus loads), because on average  $\sigma_{u,\text{obs}} \propto L_{MM}^{2/3}$  (as implied by Fig. 1 and Eqns. 9–15). Further, turbine loads are less influenced by fluctuations characterized by spatial scales significantly smaller than the blade lengths; thus the error in predicted probability for these shorter scales, and the slight underprediction of the most common  $L_{MM}$ , should not significantly influence probabilistic loads calculations relying on site-specific  $L_{MM}$  obtained via measurements and (15).

While (15) is useful to estimate  $L_{MM}$  and  $P(L_{MM})$  as shown above, one expects (13) to perform better, as it does not rely on the approximation  $c_m = \sigma_u/u_*$ . Indeed  $\langle c_m u_*/\sigma_u \rangle$  is actually 1.13 (or 1.11 (or 1.13 if considering winds down to only down to 47 m s<sup>-1</sup>) due to  $\sigma_u/u_*$  being slightly smaller and  $c_m$  slightly larger than 2.3; using these values in (13) gives estimates of  $L_{MM}$  closer to the spectrally-diagnosed  $L_{MM}$ , and within 10% of  $P(L_{MM})$  over a range of  $L_{MM}$  from below 10 m to beyond 100 m. It should also be noted that also including speeds from 7 m s<sup>-1</sup> down to 4 m s<sup>-1</sup> ignoring speeds below 7 m s<sup>-1</sup>

<sup>9</sup>The spectral fits were done using spectral-tensor model output over the parameter ranges of  $5 < L_{MM} < 500\text{ m}$  and  $0 \leq \Gamma \leq 5$ . Some spectra were poorly fitted; since these occurred when  $\Gamma = 5$ , cases with  $\Gamma > 4.95$  were excluded from the analysis here. As justification, I note that only a small fraction of the cases (< 10%) had such  $\Gamma$ , and that we only consider well-fit spectra for reliable comparison of parameters.

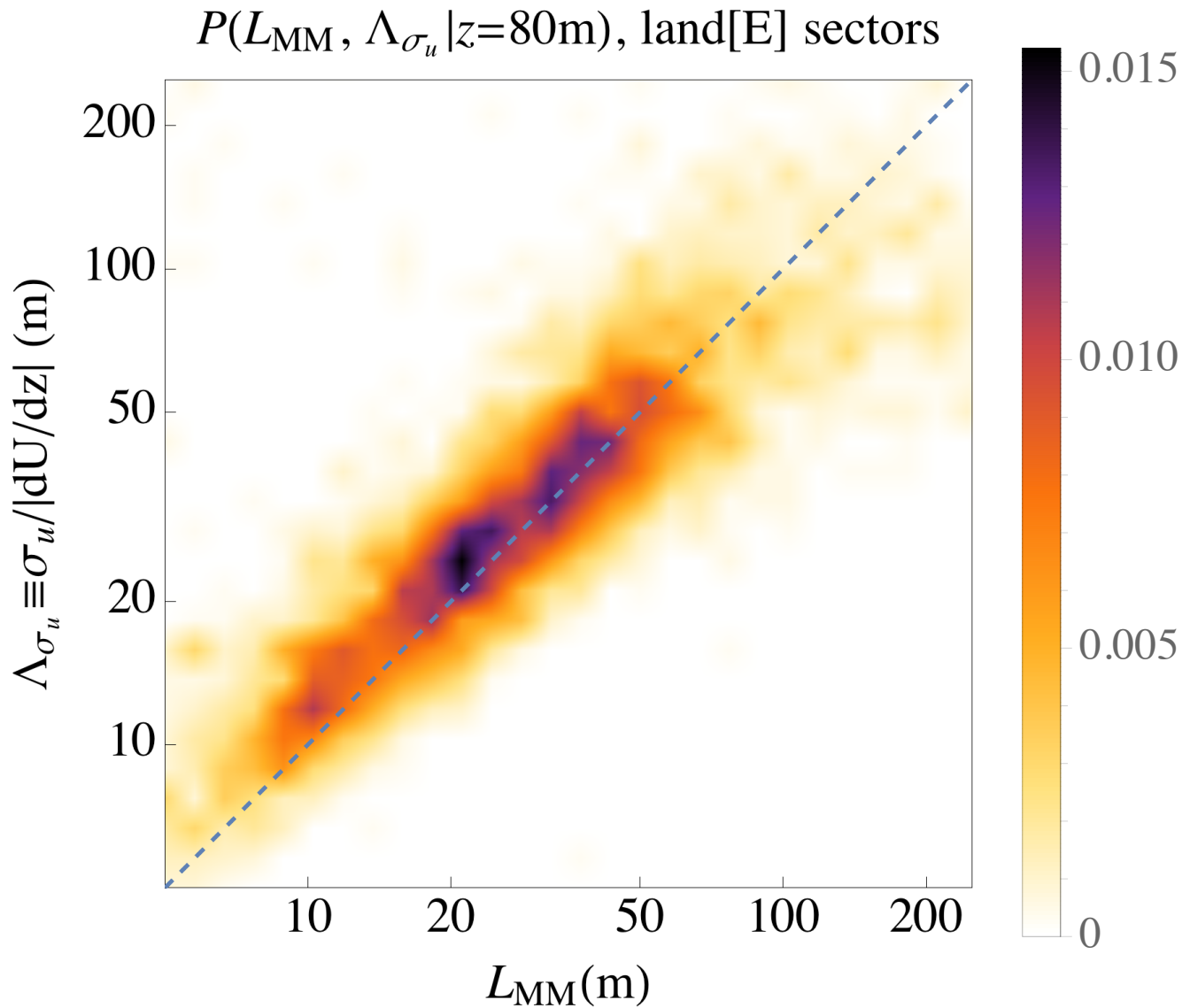


**Figure 3.** Joint probability density function of predicted and diagnosed (observed) turbulent length scale, from measurements at Høvsore over the homogeneous eastern land sectors. “*x*-axis”: Mann-model scale  $L_{\text{MM}}$  from spectral fits; “*y*-axis”:  $L_{\text{MM}}$  estimated from direct measurements of  $dU/dz$  and  $\sigma_u$ , via (15).

can lead to slightly ~~larger~~ smaller  $L_{\text{MM}}$ , since these low wind speeds are more influenced by unstable conditions. Indeed for  $L_{\text{MM}} \gtrsim 50$  m, including the lower wind speeds ~~caused~~ causes both diagnosed and predicted  $L_{\text{MM}}$  to increase roughly 10%; this is consistent with larger turbulent eddies being created under unstable conditions.

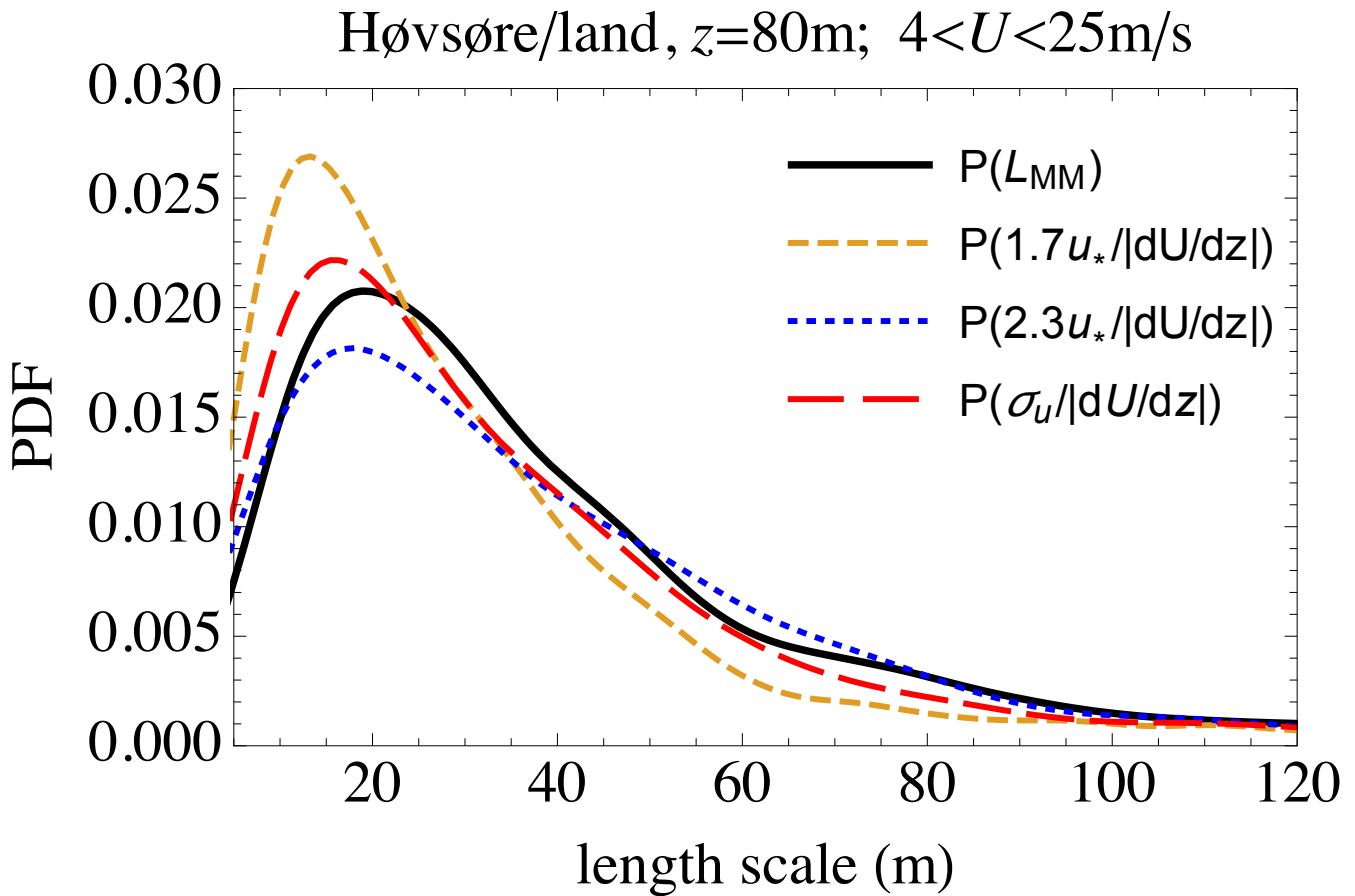


**Figure 4.** Probability density function of turbulent length scale from observations at Høvsøre from the homogeneous eastern land sectors. Black: Mann-model scale from fits to spectra; dotted/blue: ‘mixing-length’ formulation ( $\ell_m \propto u_* / |dU/dz|$ ) with revised constant; dashed/gold: Peña et al. (2010) form for  $\ell_m$ ; red/long-dashed:  $\sigma_u / |dU/dz|$  form (15).

### 3.2.1 Estimating $P(L_{MM})$ in coastal/offshore conditions

To demonstrate the (probabilistic) use of (13) or (15) for  $L_{MM}$  in somewhat different conditions, we now consider flow from offshore, using data from the same mast and height as above (Høvsøre,  $z = 80\text{ m}$ ) but for wind directions between  $240^\circ$  and  $300^\circ$ . The mast is roughly 1.75 km east of the coastline and subsequently 1.65 km east of a 16–17 m-high sand dune that lies 100 m inland, where both are locally oriented in the N-S direction (i.e. for the range of wind directions considered). The dune causes enhanced/accelerated transition of the flow from an offshore (water roughness) to an over-land flow-regime (Berg et al., 2015); this results in winds which reflect on-shore and coastal conditions at low heights (below  $\sim 40\text{--}80\text{ m}$  depending on stability) and offshore conditions at higher  $z$ .

## Høvsøre, 80m, $U=4-25\text{m/s}$

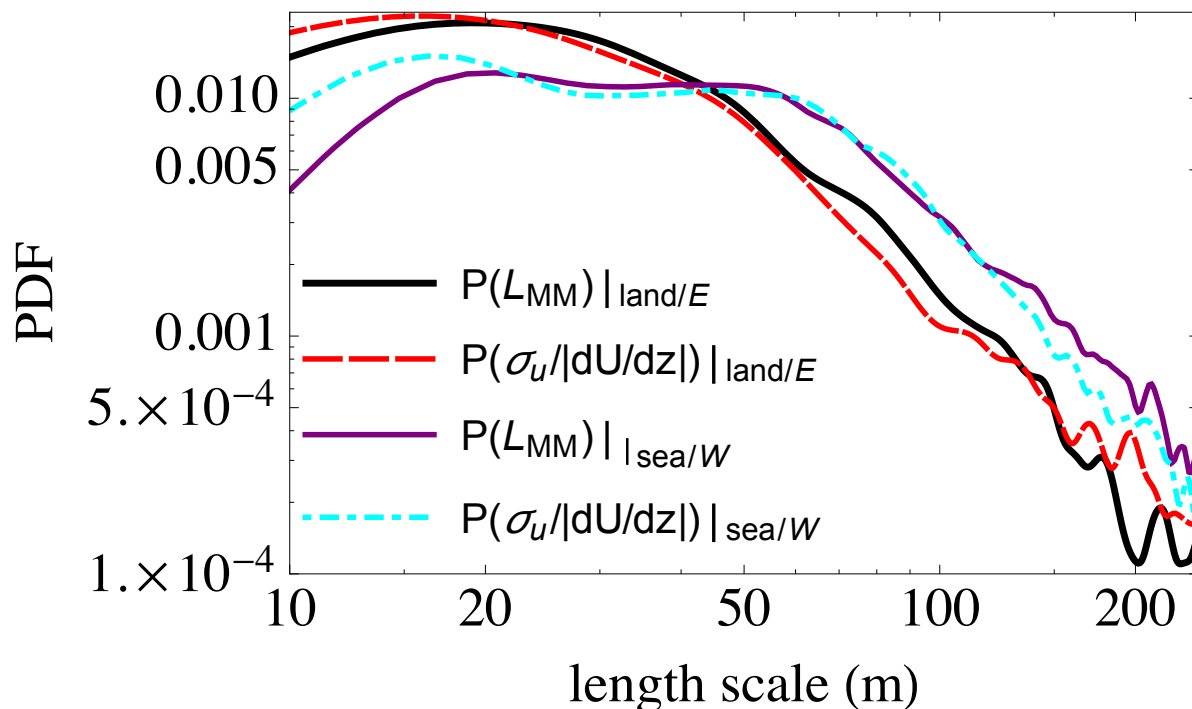


**Figure 5.** Probability density of turbulence length scale  $L_{MM}$  from observations at Høvsøre over both the homogeneous land (eastern) sectors and inhomogeneous coastal (western) sectors. Black:  $L_{MM}$  from fits to spectra over land; red/long-dashed: new simplified form (15) over land; purple:  $L_{MM}$  from fits to spectra from offshore; cyan/long-dashed-dot-dashed: new simplified form (15) from offshore.

Figure 5 displays the distribution  $P(L_{MM})$  of spectral-peak (Mann-model) length scales for coastal/offshore winds (from west  $\pm 30^\circ$ ), again using (15) to estimate  $L_{MM}$  along with  $L_{MM}$  diagnosed through spectral fits. For comparison the corresponding  $P(L_{MM})$  for easterly winds from Fig. 4 is also included. Just as for the homogeneous land case shown in Fig. 4, one sees in Fig. 5 that for inhomogeneous coastal conditions, again (15) gives  $P(L_{MM})$  basically matching the spectrally-fit observations for scales beyond  $\sim 15$  m; in this coastal regime the range of well-predicted  $L_{MM}$  extends further, to  $\sim 150$  m. While one sees that the distribution of  $L_{MM}$  is a bit different for the (western) inhomogeneous coastal case than for the (eastern) homogeneous land case, the simple expression (15) functions similarly for both flow regimes, with the arguments presented in above in section 3.2 again applying here. The  $u_*$ -based Eq. 11 also behaves similarly (not shown) as in the homogeneous land case of Fig. 4, i.e. with gross overpredictions at small scales and underpredictions at large scales. One difference between the coastal and land cases is that for small  $L_{MM}$ , (15) overestimates the distribution  $P(L_{MM})$  a bit more for the coastal regime than for the homogeneous land regime ( $L_{MM} < 20$  m); as explained above for the land case, an overprediction at the smallest is not expected to significantly impact loads calculations, due to the relatively small length scales involved.

### 3.2.2 Estimation of $P(L_{MM})$ in more complex conditions

To further show the behavior of  $L_{MM}$  and the utility of (15) at a site with more complex conditions, we examine data from the inhomogeneous forested Danish National Test Centre for Large Wind Turbines site near Østerild in Denmark (see e.g. Hansen et al., 2014, for details). Here sonic anemometer data is available at a heights of 10 m and 44 m, with concurrent data from three  
 5 lidars at  $z = \{45, 80, 140, 200, 300\}$  m. In this study we consider data from the site’s ‘western LIDAR,’<sup>10</sup> to measure winds that flow over the forest more than 70% of the time, where the canopy height is 10–20 m (Hansen et al., 2014; Sogachev et al., 2017). The analysis here uses one year (May 2010–May 2011) of wind speeds  $U \geq 5 \text{ m s}^{-1}$  from the LIDAR at 45 m and 80 m heights along with the ‘fast’ (20 Hz) data from the sonic anemometer at 44 m. The shear  $dU/dz$  is measured across 45–80 m; the spectra and subsequent turbulence/Mann-model parameters  $\{L_{MM}, \Gamma, \varepsilon\}$ , as well as and measured quantities  $\{\sigma_{u,\text{obs}}, u_{*,\text{obs}}\}$ , are  
 10 obtained from the sonic anemometer. The measurements are significantly higher than twice the forest canopy height, and thus above the roughness sublayer (Garratt, 1980; Raupach et al., 1980) and amenable to similarity and mixing-length theory (e.g. Sogachev and Kelly, 2016) as well as Mann-model use (Chougule et al., 2015).

Just as Figure 4 showed for flow over homogeneous land at Høvsøre in section 3, here Figure 6 displays the probability density of turbulence (Mann-model) length scale  $L_{MM}$  observed via spectral fits at  $z = 44$  m for Østerild, along with predictions  
 15 based on both (11) via  $u_{*,\text{obs}}$  and (15) via  $\sigma_{u,\text{obs}}$ .

As in the cases above (homogeneous land and inhomogeneous coastal), the new form (15) predicts the distribution rather well, particularly for scales between  $\sim 10$ – $100$  m—despite the shape of  $P(L_{MM})$  being different due to the trees. For the forest case of Fig. 6 the  $\sigma_u$ -based form captures both the peak (most likely  $L_{MM}$ ) and magnitude of  $P(L_{MM})$ , while the  $u_*$ -based form grossly underpredicts  $L_{MM}$ , moreso than for the previous cases. The latter is likely due to  $u_{*,\text{obs}}$  being predominantly affected  
 20 by the canopy (via ~~its~~ larger effective roughness) moreso than  $\sigma_{u,\text{obs}}$ , which tends to be more characteristic of the entire ABL (Wyngaard, 2010). There is, however a curious minor peak (with a probability ~~well under~~  $\sim 1\%$  ) for around as large as the main peak around scales of  $\sim 300 \pm 50$  m in the length-scale distribution obtained from spectral fits shown in Fig. 6, ~~which;~~ this is not captured by either ~~formulation~~ the  $u_*$ -based form (11) nor  $\sigma_u$ -based formulations (13,15). Although this peak falls spectrally at small wavenumbers (~~frequency divided by mean wind speed~~) that are more difficult to capture when spectrally  
 25 fitting the Mann model, it indeed actually corresponds to the distance to the next upwind edge of the forest (orchard segment) in the predominant wind directions.

~~Probability density function of turbulent length scale from observations at Østerild from the western mast/lidar. Black: Mann-model scale from fits to spectra; dotted-blue: ‘mixing-length’ formulation ( $\ell_m \propto u_* / |dU/dz|$ ) with revised constant; red: new form (15);  $\sigma_u / |dU/dz|$ .~~

<sup>10</sup>The ‘western LIDAR’ at Østerild is located  $\sim 1$  km west of the northern-most turbines but less than 100 m east of a forest patch and and 5–20 km from the North Sea coastline in the prevailing (W–NW) wind directions (Hansen et al., 2014).

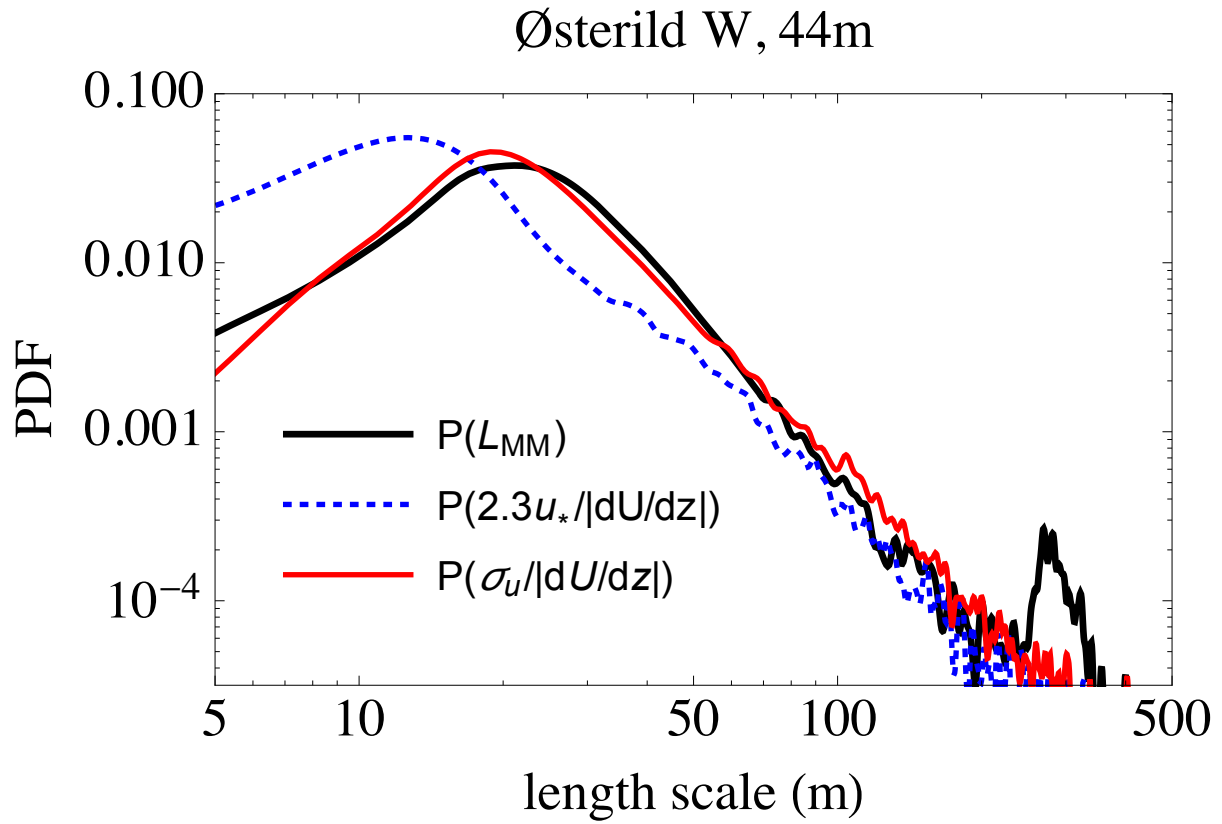


**Figure 6.** [Probability density function of turbulent length scale from observations at Østerild from the western mast/lidar. Black: Mann-model scale from fits to spectra; dotted-blue: ‘mixing-length’ formulation \( \$l\_m \propto u\_\* / |dU/dz|\$ \) with revised constant; red: new form \(15\),  \$\sigma\_u / |dU/dz|\$ .](#)

#### 4 [Discussion](#)

Towards concluding, we first revisit the motivation for (and thus context of) this work: [1] to ‘close’ the Mann (1994) eddy-lifetime ( $\tau_M$ ) formulation as implemented in rapid-distortion theory—allowing relation between Mann-model parameters ( $L_{MM}, \varepsilon, \Gamma$ ) and the shear ( $dU/dz$ ) taken to distort the modeled turbulence; [2] connect the parameters of the Mann (1994) spectral turbulence and eddy-lifetime models with atmospheric statistics, both in theory and in practice; [3] provide a formulation for the turbulence length scale  $L_{MM}$  in terms of quantities commonly-measured in wind energy; [4] demonstrate that the ‘measurable’ form developed for  $L_{MM}$  is robust and amenable to use in (probabilistic) wind turbine loads calculations. These four motivating goals have basically been realized, as shown in the previous sections, and this work has a number of implications.



## 4.1 Implications and Application

A previously suggested form (11) for  $L_{MM}$ , based on friction velocity  $u_*$  and (10-minute) mean wind shear  $dU/dz$  (Peña et al., 2010), was confirmed here to be sensitive to its proportionality constant  $c_m$ . But this constant can vary from site to site (and possibly with height), and the published value of  $c_m = 1.7$  (Peña et al., 2010) leads to significant error in prediction of  $L_{MM}$  for the different conditions (land and sea directions) at Høvsøre and at the forested site of Østerild. Finding  $c_m$  from sonic anemometer observations via  $L_{MM}$  from fits to spectra and friction velocity measurements, (11) may perform slightly better over uniform flat terrain compared to the  $\sigma_u$ -based form (15); but this can be considered a site-dependent fit in itself, as was the case when using a diagnosed value of  $c_m = 2.3$  for the homogeneous flat land sectors at Høvsøre. However, obtaining  $c_m$  is generally not possible in industrial practice; where it can be obtained, it relies on  $L_{MM}$ —which is the quantity desired—thus negating the purpose of (11). While  $u_*$  can also in principle be estimated from wind speeds taken at multiple heights by cup anemometers, this too is difficult in practice: one must account for stability, not to mention the need for measurements at multiple heights in the surface layer (or worse, the limited validity of similarity theory above the ASL). Furthermore, it is expected that  $c_m$  is a function of the (local) surface roughness, as demonstrated by the different results found over the forested Østerild site. Thus the form (15) is preferable, since it requires only the commonly-measured quantities  $\sigma_u$  and  $dU/dz$ . This simple form also gave good estimates of  $P(L_{MM})$  in the forested case—without the need for tuning, whereas the  $u_*$ -based form (11) requires a re-calculation of its coefficient  $c_m$  for such cases.

Since (13) gave yet better performance than both its simplified form (15) and the  $u_*$ -based relation (11), one might suggest its use. But (13) requires  $c_m/(\sigma_u/u_*)$ , where  $c_m$  is difficult to obtain, as discussed in the previous paragraph. However, although  $c_m$  might vary from site to site (or perhaps with height), it was found that the ratio  $c_m/(\sigma_u/u_*)$  did *not* vary appreciably—consistent with the good performance of the simplified form (15), which assumes  $c_m \approx \sigma_u/u_*$ , across sites and regimes.

One interesting implication of the testing of assumptions then follows from the finding that  $\langle \sigma_u/u_* \rangle_{\text{obs}} \approx 2.3$ , consistent in the surface-layer with Caughey et al. (1979). Examining the joint behavior of  $\sigma_u/u_*$  and the stability parameter (inverse Obukhov length)  $L^{-1}$ , the sonic anemometer data available at multiple heights in this study shows no correlation between these two quantities. The dimensionless profiles  $\sigma_u^2(z)/u_*^2 - \sigma_u^2(z)/u_{*0}^2$  and  $u_*^2(z)/u_{*0}^2$  ~~of shown by~~ Caughey et al. (1979) also imply

$$\frac{\sigma_u^2(z)}{u_*^2(z)} \approx (2.3)^2, \quad (20)$$

with the ratio ~~particularly~~ converging to a constant above the surface layer ( ~~$z/h \gtrsim 0.1$ , where  $h$  is  $z \gtrsim 0.1h$ , where~~ the atmospheric boundary-layer depth  ~~$h$  typically ranges from  $\sim 200$  m in stable conditions to 1 km or more in convective conditions~~). The flat-terrain Høvsøre data in fact show the mean value  $\langle \sigma_u/u_* \rangle_{\text{obs}}$  to be independent of  $z$ . If one knew ~~the height-dependent behavior of how~~  $c_m$  varied with height (and stability), then one could also use (20) and (13) from measurements at one height range, to estimate  $L_{MM}$  at higher  $z$ . ~~Since the the~~ (for a given stability range). Over flat terrain, on average the peak spectral scale for streamwise fluctuations ( $\lambda_u$ ) grows with  $z$  (Caughey et al., 1979; Peltier et al., 1996)<sup>11</sup>, so if we take  $L_{MM} \propto \lambda_u$  then

<sup>11</sup>The peak length scale also grows with boundary-layer depth  $h$  in convective conditions and ~~in general with decreasing (increasingly negative) thus with increasingly negative~~ inverse Obukhov length  $L^{-1}$  (e.g. Peltier et al., 1996). But over all stability conditions, which are dominated by neutral conditions

with (20) one expects the ratio  $c_m/(\sigma_u/u_*)$  to increase with  $z$  as well. Thus from (13) the Mann-model length scale  $L_{MM}$  will increase with height relative to the mixing-length  $\ell_* \equiv u_*/(dU/dz)$ , so at higher  $z$  one would expect the general form (13) to be yet more accurate than its approximate form (15); though this is not likely for wind turbine rotor heights, except in very stable conditions (Kelly et al., 2014b; Liu and Liang, 2010). Unfortunately the sonic-anemometer measurements available for this study did not include heights well beyond the surface-layer, so such variation was difficult to detect.

It is also notable that Figure 3 appears to imply the relative error (e.g. in %) in estimating  $L_{MM}$  with (15) grows for less common values of  $L_{MM}$ , particularly very large scales (and also at very small scales if including  $U < 7\text{m/s}$ , not shown). Thus (15) is recommended first for estimation of  $P(L_{MM})$ . However, the error at large scales is in part dependent on the limited (10-minute) sample lengths and the fitting routine, as there are very few points to fit at the lowest frequencies. Use of 30-minute samples can reduce such scatter, and modification of the fitting algorithms may also improve estimations of the larger scales.

Ongoing work includes wind-speed dependent prediction of  $L_{MM}$ , particularly the conditional statistics  $P(L_{MM}|U)$ . Further concurrent work also entails systematic accounting for the rotor size (shear distance) relative to height (i.e.  $\Delta z/z$ ) within the distribution of length scales; following Kelly and Gryning (2010) and Kelly et al. (2014a) a semi-empirical derivation of  $P(L_{MM})$  including  $\Delta z/z$  has been obtained, but demands more data for validation and publication. Understanding of the latter facilitates ‘vertical extrapolation’ of  $L_{MM}$  and measured turbulence and shear statistics, as well as accounting for the effect of rotor size or shear measurement span.

## 4.2 Summary of conclusions

## 5 Conclusions

- The eddy lifetime of Mann (1994), which is part of commonly used turbulence modelling for wind turbine design load cases (e.g. IEC 61400–1, Edition 3, 2005), leads to a relation for turbulence (spectral-peak) length scale  $L_{MM}$  of

$$L_{MM} \simeq \frac{c_m}{(\sigma_{u,\text{obs}}/u_{*,\text{obs}})} \frac{\sigma_u}{dU/dz},$$

where  $c_m$  and  $\sigma_{u,\text{obs}}/u_{*,\text{obs}}$  are essentially constants for a given height  $z$ , and  $c_m/(\sigma_{u,\text{obs}}/u_{*,\text{obs}})$  is found to fall between 1–1.11 for the three flow regimes analyzed.

- Theory and measurements support the assumption that  $c_m/(\sigma_{u,\text{obs}}/u_{*,\text{obs}}) \approx 1$ , roughly constant for different atmospheric flow regimes; the turbulence length scale can thus be approximated as consequently be approximated by

$$L_{MM} \simeq \frac{\sigma_u}{dU/dz};$$

thus Thus typical 10-minute mean cup anemometer measurements can be used to estimate  $L_{MM}$ .

- $L_{MM}$  is affected by atmospheric stability; this effect is contained within  $\sigma_u$  and  $dU/dz$ .

(Kelly and Gryning, 2010), and over an expected distribution of  $h$  at a given site, the basic growth of  $\lambda_u$  with  $z$  is consistent with Peltier et al. (1996) reporting  $\lambda_u \propto z$  for neutral conditions.

- In terms of the classic mixing-length form  $u_* / |dU/dz|$ , the turbulence length scale  $L_{MM}$  in the spectral-tensor model is observed to be larger (by ca. 30–40%) than previously reported by Peña et al. (2010).

*Acknowledgements.* The author thanks the reviewers for their time and effort towards constructive criticism of the present article; and thanks to Nikolay Dimitrov for discussions around probabilistic loads. This work was partly supported by the DTU Wind internally-funded cross-sectional project “*Wind to Loads*”.

## References

- Abramowitz, M. and Stegun, I. A.: Handbook of Mathematical Functions with Formulas, Graphs, and Mathematical Tables; 9th printing, Dover, New York, 1972.
- Andre, J. C. and Lesieur, M.: Influence of helicity on the evolution of isotropic turbulence at high Reynolds number, *Journal of Fluid Mechanics*, 81, 187–207, doi:10.1017/S0022112077001979, 1977.
- 5 Berg, J., Vasiljevic, N., Kelly, M. C., Lea, G., and Courtney, M.: Addressing Spatial Variability of Surface-Layer Wind with Long-Range WindScanners, *Journal of Atmospheric and Oceanic Technology*, 32, 518–527, doi:10.1175/JTECH-D-14-00123.1, 2015.
- Caughey, S., Wyngaard, J. C., and Kaimal, J.: Turbulence in the evolving stable boundary-layer, *Journal of the Atmospheric Sciences*, 36, 1041–1052, 1979.
- 10 Chougule, A., Mann, J., Segalini, A., and Dellwik, E.: Spectral tensor parameters for wind turbine load modeling from forested and agricultural landscapes, *Wind Energy*, 18, 469–481, 2015.
- Chougule, A. S., Mann, J., Kelly, M., and Larsen, G. C.: Modeling Atmospheric Turbulence via Rapid Distortion Theory: Spectral Tensor of Velocity and Buoyancy, *Journal of the Atmospheric Sciences*, 74, 949–974, doi:10.1175/JAS-D-16-0215.1, 2017.
- Comte-Bellot, G. and Corrsin, S.: Simple Eulerian time correlation of full- and narrow-band velocity signals in grid-generated, ‘isotropic’  
15 turbulence, *J. Fluid Mech.*, 48, 273–337, 1971.
- de Mare, M. T. and Mann, J.: On the Space-Time Structure of Sheared Turbulence, *Boundary-layer Meteorology*, 160, 453–474, doi:10.1007/s10546-016-0143-z, 2016.
- Dimitrov, N. K., Natarajan, A., and Kelly, M.: Model of Wind Shear Conditional on Turbulence and its impact on Wind Turbine Loads, *Wind Energy*, 18, 1917–1931, doi:10.1002/we.1797, 2015.
- 20 Dimitrov, N. K., Natarajan, A., and Mann, J.: Effects of normal and extreme turbulence spectral parameters on wind turbine loads, *Renewable Energy*, 101, 1180–1193, 2017.
- Garratt, J. R.: Surface Influence Upon Vertical Profiles in the Atmospheric Near-Surface Layer, *Quarterly Journal of the Royal Meteorological Society*, 106, 803–819, doi:10.1002/qj.49710645011, 1980.
- Hansen, B. O., Courtney, M., and Mortensen, N. G.: Wind Resource Assessment—Østerild National Test Centre for Large Wind Turbines,  
25 Tech. Rep. DTU Wind Energy E-0052(EN), Risø Lab/Campus, Danish Tech. Univ. (DTU), Roskilde, Denmark, 2014.
- IEC 61400–1, Edition 3: Wind turbine generator systems – Part 1: Safety requirements, International Electrotechnical Commission, Geneva, Switzerland, 2005.
- Kaimal, J. C., Wyngaard, J. C., Izumi, Y., and Coté, O. R.: Spectral characteristics of surface-layer turbulence, *Quart. J. Roy. Meteor. Soc.*, 98, 563–589, 1972.
- 30 Kelly, M. and Gryning, S.-E.: Long-Term Mean Wind Profiles Based on Similarity Theory, *Boundary-Layer Meteor.*, 136, 377–390, 2010.
- Kelly, M., Larsen, G., Dimitrov, N. K., and Natarajan, A.: Probabilistic Meteorological Characterization for Turbine Loads, *Journal of Physics: Conference Series*, 524, 012076, doi:10.1088/1742-6596/524/1/012076, 2014a.
- Kelly, M., Troen, I., and Jørgensen, H. E.: Weibull- $k$  revisited: ‘tall’ profiles and height variation of wind statistics, *Boundary-Layer Meteor.*, 152, 107–124, 2014b.
- 35 Lesieur, M.: *Turbulence in fluids: stochastic and numerical modelling*, Springer, doi:10.1007/978-94-009-0533-7, 1990.
- Liu, S. and Liang, X.-Z.: Observed Diurnal Cycle Climatology of Planetary Boundary Layer Height, *J. Climate*, 23, 5790–5809, 2010.
- Mann, J.: The spatial structure of neutral atmospheric surface-layer turbulence, *J. Fluid Mech.*, 273, 141–168, 1994.

- Mann, J.: The spectral velocity tensor in moderately complex terrain, *J. Wind Eng.*, 88, 153–169, 2000.
- Mann, J., Ott, S., Jørgensen, B. H., and Frank, H. P.: WASP Engineering 2000, Tech. Rep. Risø-R-1356(EN), Risø National Laboratory, Roskilde, Denmark, 2002.
- Mann, J., Astrup, P., Jensen, N., Landberg, L., and Jørgensen, H.: The meteorology of ‘the very large wind turbines’, in: Proc. of the 2004  
5 European Wind Energy Conference, European Wind Energy Association (EWEA), London, 2005.
- Peña, A., Gryning, S.-E., and Mann, J.: On the length-scale of the wind profile, *Royal Meteorological Society. Quarterly Journal*, 136, 2119–2131, 2010.
- Peña, A., Floors, R. R., Sathe, A., Gryning, S.-E., Wagner, R., Courtney, M., Larsén, X. G., Hahmann, A. N., and Hasager, C. B.: Ten Years  
10 of Boundary-Layer and Wind-Power Meteorology at Høvsøre, Denmark, *Boundary-layer Meteorology*, 158, 1–26, doi:10.1007/s10546-015-0079-8, 2016.
- Peltier, L. J., Wyngaard, J. C., Khanna, S., and Brasseur, J. G.: Spectra in the Unstable Surface Layer, *J. Atmos. Sci.*, 53, 49–61, 1996.
- Pope, S. B.: *Turbulent Flows*, Cambridge University Press, 2000.
- Raupach, M., Thom, A., and Edwards, I.: A Wind-Tunnel Study of Turbulent-Flow Close to Regularly Arrayed Rough Surfaces, *Boundary-layer Meteorology*, 18, 373–397, doi:10.1007/BF00119495, 1980.
- 15 Sathe, A., Mann, J., Barlas, T. K., Bierbooms, W., and van Bussel, G.: Influence of atmospheric stability on wind turbine loads., *Wind Energy*, 16, 1013–1032, 2013.
- Savill, A. M.: Recent developments in rapid-distortion theory, *Annu. Rev. Fluid Mech.*, 19, 531–575, 1987.
- Sogachev, A. and Kelly, M.: On Displacement Height, from Classical to Practical Formulation: Stress, Turbulent Transport and Vorticity Considerations, *Boundary-Layer Meteorology*, 158, 361–381, doi:10.1007/s10546-015-0093-x, 2016.
- 20 Sogachev, A., Cavar, D., Kelly, M., and Bechmann, A.: Effective roughness and displacement height over forested areas, via reduced-dimension CFD, Tech. Rep. DTU Wind Energy E-0161(EN), Risø Lab/Campus, Danish Technical University (DTU), Roskilde, Denmark, 2017.
- von Kármán, T.: Progress in the Statistical Theory of Turbulence, *Proceedings of the National Academy of Sciences*, 34, 530–539, doi:10.1073/pnas.34.11.530, 1948.
- 25 Wyngaard, J. C.: *Turbulence in the Atmosphere*, Cambridge University Press, 2010.